JOURNAL OF MATERIALS SCIENCE 24 (1989) 1383–1388

Effects of composition and thickness on the electrical properties of indium oxide/tin oxide multilayered films

TAKEYUKI SUZUKI, TSUTOMU YAMAZAKI, HARUNOBU ODA
Department of Industrial Chemistry, Faculty of Technology, Tokyo University of Agriculture and Technology, Koganei, Tokyo 184, Japan

Indium oxide/tin oxide multilayered films with a 2 nm pair thickness were deposited on glass substrates at temperatures lower than 100° C by an ion-beam sputtering method. The structure, electrical properties and visible transmissivity were investigated as a function of composition and the total thickness on as-deposited and annealed films. X-ray diffraction analysis showed that the as-deposited 200 nm thick film (with 0.15 nm tin oxide layers) was partially crystalline and films thinner than 100 nm were amorphous or microcrystalline. The room-temperature resistivity of as-prepared films increased with the increase of an average tin oxide layer thickness from ~0.05 to ~0.3 nm (ideal monolayer thickness) under a constant total thickness ~100 nm. We observed a decrease of the Hall mobility with the increase of the total film thickness from 10 to 200 nm in as-deposited samples containing 0.15 nm tin oxide layers.

1. Introduction

Low-temperature fabrication of indium tin oxide (ITO) films can be applied for transparent and protective electrodes and also for heat-reflecting mirrors on amorphous semiconductors or even on plastic films without deteriorating them thermally. Thus a variety of low-temperature synthesis of the ITO films has been reported. For example, Itoyama [1] has deposited films on Pyrex glasses at low temperatures (140 to 180° C) by r.f. sputtering using an In_2O_3–5 wt % SnO_2 target. The structure of the as-deposited films (400 to 500 nm thick) was amorphous-like and the room-temperature (RT) resistivities were in the range (1 to 2) × 10^{-3} Ω cm at a deposition rate lower than ~3 nm sec^{-1}.

Itoyama [2] has further shown that coatings on polyester films at high rates (2 to 8 nm sec^{-1}) exhibited nearly the same optical properties as those formed on glass substrates by high-temperature processes. Fan [3] has made amorphous (or very finely polycrystalline) films on both glass and Mylar substrates by the ion-beam sputtering (IBS) method using an In_2O_3–12 mol % SnO_2 target at deposition temperatures below 100° C; the deposition rate was ~0.3 nm sec^{-1}. These films (500 to 600 nm thick) showed low RT resistivities (~5.5 × 10^{-4} Ω cm) and high visible transmission (> 80%) provided that the oxygen partial pressure was maintained at (2 to 3) × 10^{-5} torr.

Shewchun *et al.* [4] have deposited films on glass slides by the IBS method prior to the fabrication of ITO (400 nm)/p-Si single-crystal solar cells; the best photovoltaic devices were obtained from the In_2O_3–9 mol% SnO_2 target composition. The majority of the films on glass slides exhibited an as-sputtered resistivity of (3 to 7) × 10^{-4} Ω cm and high transparency.

Howson *et al.* [5] have produced films by the reactive ion plating of In–10% Sn on to glass and plastic substrates at room temperature. They showed that the carrier densities decreased and the mobilities increased with increased film thickness from 100 to 500 nm. Films deposited on to polyester sheet were crystalline with a crystal size of around 10 nm. Buchanan *et al.* [6] have prepared 80 nm films by magnetron sputtering at low temperatures (40 to 180° C). They observed a low room-temperature (RT) resistivity (~4 × 10^{-4} Ω cm) and high visible transmission (> 85%) with an oxygen partial pressure of (2 to 7) × 10^{-5} torr.

Nath *et al.* [7] have reactively evaporated films on glasses in the presence of Ar–15% O_2 at the deposition rate of 0.67 nm sec^{-1}. Films prepared on room-temperature substrates from the In–18 wt % Sn showed an RT resistivity of the order of 1 Ω cm and a transmittance higher than 90%. They observed that these films have no discernible microstructure and thought that low deposition temperatures led to stoichiometric oxide films.

Naseem and Coutts [8] have r.f. sputter deposited films from a target of In_2O_3–10 mol % SnO_2; the substrate temperatures did not exceed 50° C. Films deposited very slowly (~0.03 nm sec^{-1}) in argon had a very high resistivity and the post-deposition annealing could not reduce the resistivity to less than 10^{-2} Ω cm. They found that films made in a mixture of Ar–10% H_2 gas reduced the RT resistivity to less than 2 × 10^{-3} Ω cm, independent of the deposition rate.

Films have also been prepared at a rate ~0.2 nm sec^{-1} by oxygen ion-assisted deposition using an In_2O_3–9 mol % SnO_2 target by Martin *et al.* [9]. Transmission electron microscopy revealed that the 20 nm thick films on ambient temperature substrates were

0022–2461/89 $03.00 + .12

mostly amorphous. X-ray diffraction studies of thicker films prepared at a substrate temperature of 100° C showed the cubic In_2O_3 structure; the crystal sizes were estimated to be ~20 nm. The RT electrical resistivity of films 135 nm thick decreased from $\sim 1 \times 10^{-2}\,\Omega$cm for layers deposited on to room-temperature substrates to around $5 \times 10^{-3}\,\Omega$cm at 100° C.

Banerjee *et al.* [10] have deposited films at 50° C directly on to carbon-coated copper microgrids by magnetron sputtering. The electron diffraction pattern revealed the crystalline nature of the ~8 nm thick films; however, the corresponding micrograph did not show detectable microstructure. The micrograph of the 30 nm thick film showed the average grain size varying between 10 and 30 nm. The visible transmittance was nearly invariant for the thickness range 30 to 300 nm; there was no significant change in the carrier concentration between films of thickness 30 to 150 nm.

Other topics relating to the ITO films have been reviewed by Chopra *et al.* [11] and Hamberg and Granqvist [12].

In a previous work [13], we proposed a new fabrication method. The repeated alternate deposition of thin layers of indium oxide (InO_x) and tin oxide (SnO_y) gave rise to optically transparent and electrically conducting multilayered films whose properties were comparable or superior to those of conventional ITO films. The work reported here is a natural extension of the previous work. The influence of composition and the total film thickness upon the electrical and optical properties of InO_x/SnO_y multilayered films is described.

2. Experimental methods

The films were prepared using an IBS apparatus with a beam-power voltage of 1000 or 500 V and an accelerator voltage of 150 V. The targets, In_2O_3 (99.99% purity) and SnO_2 (99.99% purity), were sputtered alternately with an argon ion-beam under a vacuum of 1×10^{-4} torr. The substrate temperature was always lower than 100° C during sputtering. Details of the sputtering method have been described elsewhere [14]. The films were deposited on optical-flat glass substrates; Pyrex for electrical measurement and fused quartz for optical measurement. The in-plane electrical resistivity of the films was measured in air by the Van der Pauw method with platinum electrodes formed by the IBS technique. The carrier concentration, n, and the Hall mobility, μ_H, were measured under a d.c. magnetic field of 5500 G. The film thickness analysis, X-ray diffraction analysis, heat-treatment and optical measurement were the same as described previously [13].

As illustrated in Fig. 1, the geometry of a multilayered film is specified by a layer thickness of indium oxide $d(InO_x)$, that of tin oxide $d(SnO_y)$ and the total film thickness L; a pair thickness d is equal to $d(InO_x) + d(SnO_y)$ and L/d gives the pair number. We will designate a multilayered film as "$d(InO_x)/d(SnO_y) \times L/d$" here. Thus "1.85/0.15 × 50" means, for example, that the multilayered film consists of 50 pairs of a 1.85 nm InO_x layer and a 0.15 nm SnO_y layer.

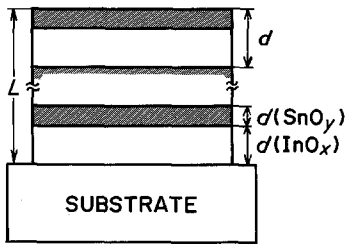

Figure 1 Schematic illustration of the geometry of a multilayered film.

3. Results and discussion

3.1. Film thickness and structure

Two deposition rates, high and low, were used. The low deposition rate of indium oxide and tin oxide was 0.012 and 0.027 nm sec^{-1}, respectively. In this section, only the high deposition rate is discussed; the method of determining the rate is always the same. The sputtering time of tin oxide was set to 20 sec and that of indium oxide was varied from 50 to 400 sec. The pair thickness, d, can be calculated using the Bragg equation

$$d_{n,n+1} = \frac{\lambda}{2}\left(\frac{2n+1}{\sin^2\theta_{n+1} - \sin^2\theta_n}\right)^{1/2} \quad (1)$$

where θ_n is the diffraction angle from the nth reflection and λ is the X-ray wavelength (0.154 nm).

Fig. 2 shows the pair thickness as a function of the sputtering time of indium oxide. The gradient of the straight line gives the deposition rate of the indium oxide to be 0.034 nm sec^{-1}; interpolation of the plots to the pair thickness axis shows a deposition rate of 0.074 nm sec^{-1} of the tin oxide. This higher deposition rate thus obtained was then used to design multilayered films with a 2 nm pair thickness series such as 1.85/0.15 × 1, × 2, × 5, × 10, × 20, × 50 and × 100. It is to be noted that the real $d(SnO_y)$ is slightly thicker than 0.15 nm, because the SnO_2 target is sputtered during the rotation whose rate is about 0.6 sec/90°.

The electrical and optical properties of these films are discussed in the following sections, but first let us look at the total film thickness. It is seen that Equation 1 also holds for the total film thickness $L_{m,m+1}$; an

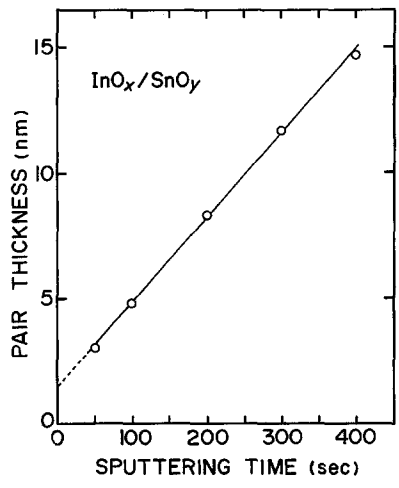

Figure 2 Pair thickness, d, as a function of the sputtering time of indium oxide. Tin oxide was always sputtered for 20 sec.

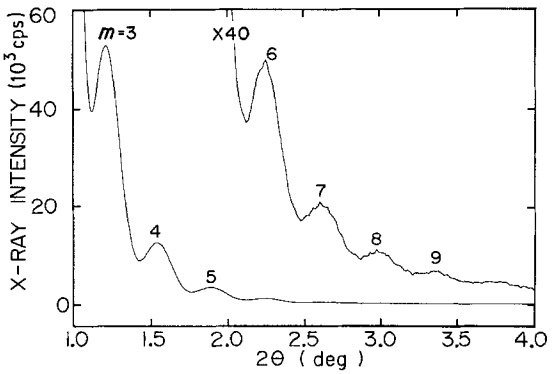

Figure 3 Low-angle X-ray diffraction pattern from the total film thickness. The chart shows that the actual thickness, $L \sim 23$ nm, is slightly larger than the designed value of 20 nm.

example of a designed thickness $L = 20$ nm with $d = 2$ nm is shown in Fig. 3. Here we see reflection only from the total thickness, L, and no peak originating from the pair thickness, d. Applying the equation for $L_{m,m+1}$ to the film, it was found that the actual average thickness was 22.7 nm, 14% thicker than the designed value. The same was true for the designed 40 nm film; the actual value was 45.0 nm, about 13% thicker than expected. This discrepancy probably arises mainly from mis-setting of the targets in a different series of sample preparation. Detailed calculations including the refraction correction ignored in Equation 1 are discussed by Underwood and Barbee [15]. However, this simple and approximate method of calculating the total film thickness is useful for obtaining a rough deposition rate of a single layer, at least in the first stage of an experiment.

Next, the structure of as-deposited films was examined. Fig. 4 shows typical examples of the X-ray diffraction patterns. The 200 nm film (1.85/0.15 × 100) is partially crystallized to the cubic In_2O_3 (JCPDS 6-0416); however, the 100 nm film (1.85/0.15 × 50) is amorphous or microcrystalline. Other films with $d = 2$ nm, $d(SnO_y) = 0.15$ nm and $L \leqslant 100$ nm were all amorphous (or microcrystalline). Such an amorphous–crystalline transition with increasing film thickness has also been reported in undoped-indium oxide by Muranaka *et al.* [16]. They evaporated films (2.5 to 30 nm thick) on to SiO at 150° C at a rate of 0.1 nm sec^{-1}. The electron diffraction and micrograph studies revealed that the 2.5 nm film was mainly amorphous with a number of small crystallites of 10 nm or less in size. These crystallites grew with increased film thickness and the 30 nm film became entirely composed of crystallites of mean size about 140 nm. Banerjee *et al.* [10] reported similar dependence of crystallization on the film thickness. Our observation indicates that the local composition of our films is almost "homogeneous" and that the 1.85 nm layers of indium oxide are not clearly separated by the tin oxide layers. In other words, the designed $d(SnO_y) = 0.15$ nm layer is too thin to form a layer, because the ionic radii of Sn^{4+} and O^{2-} are 0.069 and 0.14 nm, respectively [17]. A rough geometrical estimation shows that about one-half of the adjacent indium oxide layers are interconnected and only the other half are separated by a tin oxide layer.

3.2. Composition and electrical properties

The composition of a film is given here as a thickness ratio $d(SnO_y)/d(InO_x)$ of an as-deposited film. In our previous work [13], properties of films with a fixed composition $d(SnO_y)/d(InO_x) \sim 0.1$ were studied as a function of the pair thickness, d. As a result, a low resistivity of $\sim 1 \times 10^{-3}$ Ω cm was found in films with $d = 1.1$ and 2.2 nm in their as-prepared and annealed state. Films with $d = 5.7$ and 11.4 nm showed an inferior conductivity when annealed at 300° C for longer than 0.5 h. Thus we examine here electrical properties of the $d = 2$ nm films as a function of composition, namely, films with $d(SnO_y) = 0$, 0.05, 0.1, 0.15, 0.2, 0.25, 0.3, 0.35, 0.4 and 0.6 nm; L is kept constant to ~ 100 nm. This series of films was made using the low deposition rates of 0.012 nm sec^{-1} for indium oxide and 0.027 nm sec^{-1} for tin oxide.

Fig. 5 shows the RT resistivity of as-deposited and annealed films (five or six samples) and Fig. 6 shows the corresponding Hall mobility, μ_H, and the carrier

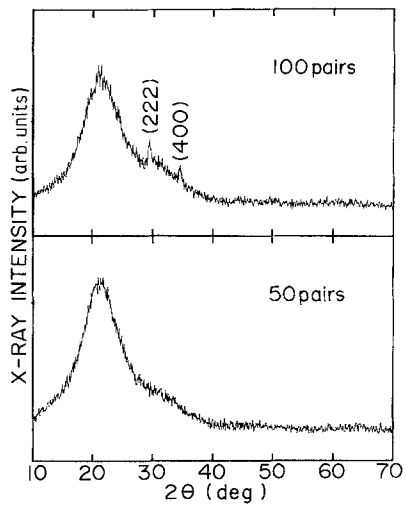

Figure 4 Typical examples of X-ray diffraction patterns from the as-prepared InO_x/SnO_y multilayered films with $d = 2$ nm and $d(SnO_y) = 0.15$ nm. Thicker film ($L = 200$ nm) is partially crystalline in the cubic In_2O_3 form, whereas thinner film ($L = 100$ nm) is amorphous or microcrystalline.

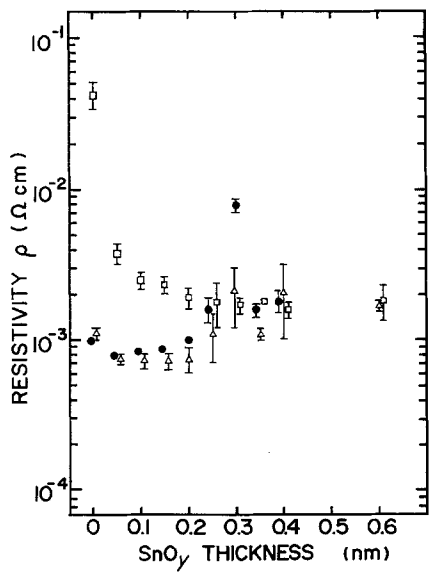

Figure 5 Room-temperature in-plane resistivity, ϱ, of the $d = 2$ nm films with varying $d(SnO_y)$ from 0 to 0.6 nm. L is kept constant to ~ 100 nm. (●) As-deposited; (△) 200° C, 5 h; (□) 300° C, 5 h.

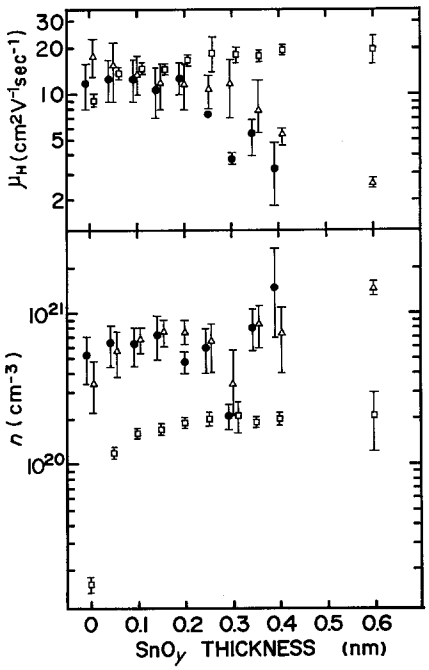

Figure 6 Hall mobility, μ_H, and carrier concentration, n, of films corresponding to those of Fig. 5. (●) As-deposited; (△) 200° C, 5 h; (□) 300° C, 5 h.

(electron) concentration, n. The electrical properties of films annealed at 100° C for 5 h are not given here, because they showed almost the same behaviour as those annealed at 200° C for 5 h except for the $d(SnO_y) = 0.3$ nm films. The lowest resistivity in an as-deposited film, $\varrho = 7.4 \times 10^{-4}\,\Omega$cm, was obtained at the composition $d(SnO_y) = 0.05$ nm. At this composition, a homogeneous SnO_y layer is not yet fomed and the tin atoms are randomly distributed on planes. Thus the film structure may be regarded as an "ordered amorphous solid". The nature of the "ordered amorphous solid" increases with the increasing $d(SnO_y)$, at least up to a thickness corresonding to one homogeneous SnO_y layer; that is around 0.28 nm, the diameter of an oxygen ion. Fig. 7 illustrates schematically the apparent layer thickness $d(SnO_y)$ and the

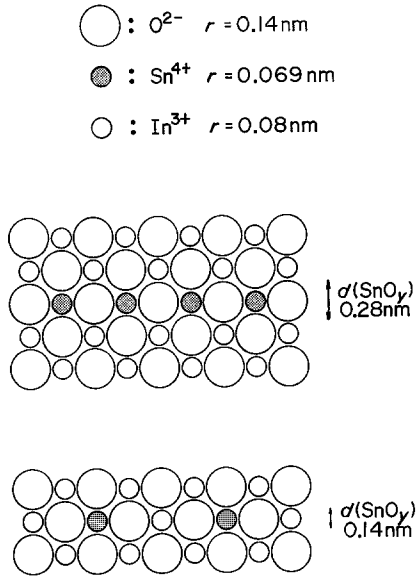

Figure 7 An atomistic representation of the tin oxide layer thickness $d(SnO_y)$. Ideal monolayer occurs at the diameter of the oxygen ion, 0.28 nm. When $d(SnO_y)$ is less than 0.28 nm, the tin oxide layer becomes discontinuous.

distribution of tin atoms. It is rather surprising that the as-deposited $d(SnO_y) = 0.3$ nm films exhibit higher resistivity $(8.1 \pm 0.6) \times 10^{-3}\,\Omega$cm, compared to films with adjacent composition; films annealed at 100° C for 5 h also showed a high resistivity of $(8.4 \pm 1.3) \times 10^{-3}\,\Omega$cm. As Fig. 6 indicates, this peak comes mainly from the sudden decrease in the carrier concentration; further study of this phenomenon is underway.

Films annealed at 200° C for 5 h exhibited similar electrical properties between $d(SnO_y) = 0.05$ and 0.2 nm. Typically, they are $\varrho = (6 \text{ to } 8) \times 10^{-4}\,\Omega$cm, $\mu_H = 8$ to $22\,cm^2\,V^{-1}\,sec^{-1}$ and $n = (4 \text{ to } 9) \times 10^{20}\,cm^{-3}$. The minimum resistivity, $5.7 \times 10^{-4}\,\Omega$ cm, is obtained in a $d(SnO_y) = 0.15$ nm film with $\mu_H = 17\,cm^2\,V^{-1}\,sec^{-1}$ and $n = 6.4 \times 10^{20}\,cm^{-3}$. When annealed at 300° C for 5 h, the higher resistivity at $d(SnO_y) = 0.3$ nm ceased to exist, this is probably because the diffusion destroyed the homogeneous SnO_y layer and produced a film resembling a solid solution. The resistivity became nearly forty times higher at the pure InO_x side and decreased with the increasing $d(SnO_y)$ reaching a constant value, $\sim 2 \times 10^{-3}\,\Omega$cm, at $d(SnO_y) \geqslant 0.2$ nm. Higher resistivity at $d(SnO_y) \leqslant 0.2$ nm is due to reduced carrier concentration; effects of increased mobility and decreased carrier concentration cancelled out at $d(SnO_y) \geqslant 2.5$ nm.

Although the detailed mechanism of the electrical properties in tin-doped indium oxide is not well understood, it is generally recognized that oxygen vacancies play an important role [18–20]. Here we consider only two kinds of defects using Kröger–Vink notation [21]; they are $V_O^{\cdot\cdot}$ and $Sn_{In}^{\cdot}$. Our observation indicates that the doubly charged donors $V_O^{\cdot\cdot}$ in as-deposited films markedly diminished (leading to a reduction of the carrier concentration) when annealed at 300° C for 5 h in air

$$V_O^{\cdot\cdot} + 2e' + \tfrac{1}{2}O_2(g) \rightarrow O_O^{\times}$$

This appeared typically in undoped-indium oxide films. Contrary to this reduction of conduction electrons, the diffusion of cations increases the carriers, because the thermal migration of Sn^{4+} produces the singly charged donners $Sn_{In}^{\cdot}$. Figs 5 and 6 show that these chemical reactions occurred when annealed at 300° C for 5 h. It is probable that annealing at 200° C for 5 h mainly diminished the mechanical stresses of the films, without accompanying the above chemical reactions, leading to a slight amelioration of the electrical properties.

Let us now examine the mean free path [22], l, of the carriers to obtain an insight into the scattering mechanism.

$$l = \left(\frac{h}{2e}\right)\left(\frac{3n}{\pi}\right)^{1/3}\mu$$

We calculate the two typical examples; one is the as-deposited film of $d(SnO_y) = 0.3$ nm having the highest resistivity and the other is the $d(SnO_y) = 0.15$ nm film annealed at 200° C for 5 h which exhibited the minimum resistivity. The former yielded $l \sim 0.46$ nm with $n = 2.1 \times 10^{20}\,cm^{-3}$ and $\mu_H = 3.8\,cm^2$

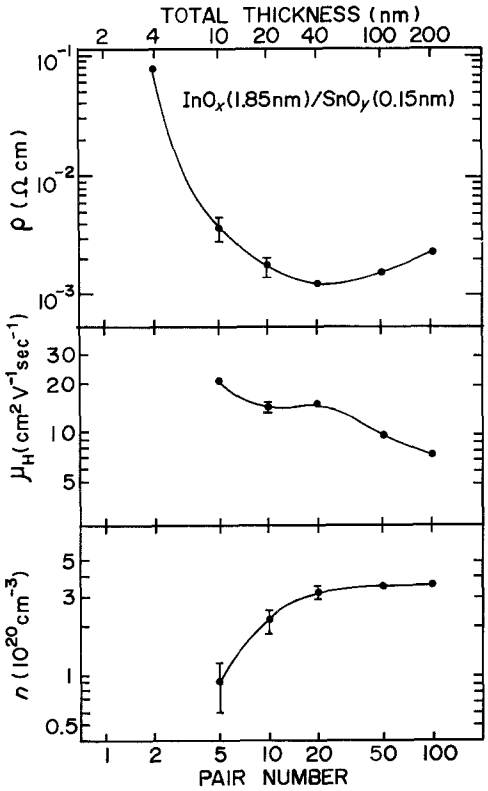

Figure 8 Room-temperature in-plane resistivity, ϱ, Hall mobility, μ_H, and carrier concentration, n, of the as-prepared $d = 2$ nm films with $d(SnO_y) = 0.15$ nm as a function of the pair number.

$V^{-1} sec^{-1}$; the latter proved to be $l \sim 3.0$ nm with $n = 6.4 \times 10^{20} cm^{-3}$ and $\mu_H = 17 cm^2 V^{-1} sec^{-1}$. The former mean free path, 0.46 nm, is considerably shorter than a layer thickness of $d(InO_x) = 1.7$ nm and is comparable to the distance between atoms. This is known to occur particularly in non-crystalline materials [23]. On the other hand, the latter value, $l \sim 3.0$ nm, although too long compared to the $d(InO_x) = 1.85$ nm, seems to suggest scattering due to an ordered structure such as the layered or crystalline nature of the film.

3.3. Influence of total film thickness

The electrical and optical properties of the $d = 2$ nm films with $d(SnO_y) = 0.15$ nm were examined as a function of the pair number L/d, because this composition has the minimum resistivity when annealed at 200° C for 5 h, as shown in the preceeding section. Fig. 8 shows the RT electrical resistivity, Hall mobility and the carrier (electron) concentration in air. A sharp increase in resistivity with the decrease of the film thickness is often observed for ITO films [10, 24] and also for In_2O_3 films [25–27]. The origin of the present sharp increase lies in the decrease of the carrier concentration, which is probably induced by the chemisorption of oxygen. On the other hand, a slight increase in resistivity from 40 to 200 nm can be attributed to the reduction of the Hall mobility.

A similar resistivity minimum around the thickness of 50 nm is also reported in amorphous SnO_x films [28]. The Hall mobility decreased with increased film thickness from 10 to 200 nm. Although few reports are available on the mobility of semiconducting oxides as a function of submicrometre thickness, the general trend is increased mobility with film thickness [5, 24, 29–32]. In fact, undoped-indium oxide films prepared by the present IBS method showed, contrary to our present observation, an increased Hall mobility from ~ 3 to $\sim 10 cm^2 V^{-1} sec^{-1}$ with increased thickness from 5.2 to 113 nm [33]. Thus the decreasing Hall mobility with thickness originates probably from the inserted discontinuous tin oxide layer between the indium oxide (Fig. 7). We postulate that an InO_x/SnO_y multilayer film has a large residual stress and that of pure InO_x film is negligibly small; the spontaneous stress relaxation in thinner multilayered films results in a higher mobility than of unrelaxed thicker films.

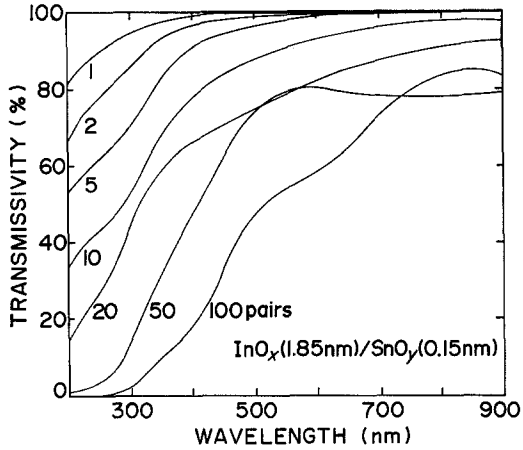

Figure 9 Visible transmissivity of the as-prepared $d = 2$ nm films having $d(SnO_y) = 0.15$ nm with varying pair number.

It should be noted that Rutledge [34] reports an increased electrical resistance with mechanical tension in ITO films. The influence of the total film thickness (or pair number) on the visible transmissivity is given in Fig. 9. Evidently, thinner films showed a better transmissivity, T; $T \gtrsim 80\%$ for films thinner than ~ 100 nm.

4. Conclusions

1. Low-angle X-ray diffraction showed reflection peaks from the total film thickness ranging from 10 to 40 nm.
2. The 200 nm film was partially crystalline, however, films thinner than 100 nm were amorphous or microcrystalline.
3. The resistivity of the multilayered film increased with increasing SnO_y layer thickness from 0.05 to 0.3 nm.
4. The minimum resistivity, $5.7 \times 10^{-4} \Omega cm$, was obtained for films with the 0.15 nm SnO_y layer thickness when annealed at 200° C for 5 h in air.
5. The Hall mobility decreased and the carrier (electron) concentration increased with the total film thickness.

Acknowledgement

We thank Professor N. Oyama, Department of Applied Chemistry for Resources, for help with film thickness analysis.

References

1. K. ITOYAMA, *Jpn J. Appl. Phys.* **17** (1978) 1191.
2. *Idem, J. Electrochem. Soc.* **126** (1979) 691.

3. J. C. C. FAN, *Appl. Phys. Lett.* **34** (1979) 515.
4. J. SHEWCHUN, J. DUBOW, C. W. WILMSEN, R. SINGH, D. BURK and J. F. WAGER, *J. Appl. Phys.* **50** (1979) 2832.
5. R. P. HOWSON, J. N. AVARITSIOTIS, M. I. RIDGE and C. A. BISHOP, *Thin Solid Films* **63** (1979) 163.
6. M. BUCHANAN, J. B. WEBB and D. F. WILLIAMS, *Appl. Phys. Lett.* **37** (1980) 213.
7. P. NATH, R. F. BUNSHAH, B. M. BASOL and O. M. STAFFSUD, *Thin Solid Films* **72** (1980) 463.
8. S. NASEEM and T. J. COUTTS, *ibid.* **138** (1986) 65.
9. P. J. MARTIN, R. P. NETTERFIELD and D. R. McKENZIE, *ibid.* **137** (1986) 207.
10. R. BANERJEE, S. RAY and A. K. BARUA, *J. Mater. Sci. Lett.* **6** (1987) 1203.
11. K. L. CHOPRA, S. MAJOR and K. PANDYA, *Thin Solid Films* **102** (1983) 1.
12. I. HAMBERG and C. G. GRANQVIST, *J. Appl. Phys.* **60** (1986) R123.
13. T. SUZUKI, T. YAMAZAKI and H. ODA, *J. Mater. Sci.* **23** (1988) 3026.
14. T. SUZUKI, T. YAMAZAKI, T. TAKAHASHI, T. KAGEYAMA and H. ODA, *J. Mater. Sci. Lett.* **7** (1988) 79.
15. J. H. UNDERWOOD and T. W. BARBEE Jr, *Appl. Optics* **20** (1981) 3027.
16. S. MURANAKA, Y. BANDO and T. TAKADA, *Thin Solid Films* **151** (1987) 355.
17. R. D. SHANNON, *Acta Crystallogr.* **A32** (1976) 751.
18. G. FRANK and H. KÖSTLIN, *Appl. Phys.* **A27** (1982) 197.
19. J. C. MANIFACIER, L. SZEPESSY, J. F. BRESSE, M. PEROTIN and R. STUCK, *Mater. Res. Bull.* **14** (1979) 163.
20. J. C. C. FAN and J. B. GOODENOUGH, *J. Appl. Phys.* **48** (1977) 3524.
21. F. A. KRÖGER, "The Chemistry of Imperfect Crystals", Vol. II (North-Holland, Amsterdam, 1974) p. 1.
22. S. NOGUCHI and H. SAKATA, *J. Phys. D Appl. Phys.* **13** (1980) 1129.
23. N. F. MOTT, "Metal-Insulator Transitions" (Taylor and Francis, London, 1974) p. 26.
24. S-W. JAN and S-C. LEE, *J. Electrochem. Soc.* **134** (1987) 2056.
25. C. A. PAN and T. P. MA, *Appl. Phys. Lett.* **37** (1980) 163.
26. *Idem, J. Electrochem. Soc.* **128** (1981) 1953.
27. D. LASER, *J. Appl. Phys.* **52** (1981) 5179.
28. T. SUZUKI and T. YAMAZAKI, *J. Mater. Sci. Lett.* **6** (1987) 1086.
29. H. D. WAAL and F. SIMONIS, *Thin Solid Films* **77** (1981) 253.
30. H. KANEKO and K. MIYAKE, *J. Appl. Phys.* **53** (1982) 3629.
31. S. MAJOR, A. BANERJEE, K. L. CHOPRA and K. C. NAGPAL, *Thin Solid Films* **143** (1986) 19.
32. W. S. LAU and S. J. FONASH, *J. Electron. Mater.* **16** (1987) 141.
33. T. SUZUKI, T. YAMAZAKI, M. TAKIZAWA and O. KAWASAKI, *J. Mater. Sci.* **23** (1988) in press.
34. S. K. RUTLEDGE, "Thin Films-Interface and Phenomena" (Materials Research Society, Pittsburgh, Pennsylvania, 1986) p. 187.

Received 1 March
and accepted 25 July 1988